International Journal of Fatigue 97 (2017) 135–149

Contents lists available at ScienceDirect

International Journal of Fatigue

journal homepage: www.elsevier.com/locate/ijfatigue

An investigation on crack growth rate of fatigue and induction heating thermo-mechanical fatigue (TMF) in Hastelloy X superalloy via LEFM, EPFM and integration models

M. Esmaeilzadeh [a], F. Qods [a,*], H. Arabi [b], B.M. Sadeghi [b]

[a] Faculty of Metallurgical and Materials Engineering, Semnan University, Semnan, Iran
[b] School of Metallurgy and Materials Engineering, Iran University of Science & Technology, Tehran, Iran

ARTICLE INFO

Article history:
Received 10 October 2016
Received in revised form 22 December 2016
Accepted 24 December 2016
Available online 28 December 2016

Keywords:
Thermo-mechanical fatigue
Crack growth rate
Induction heating
Pure fatigue
Cyclic creep
Induced eddy currents
Crack healing

ABSTRACT

In this research, fatigue and induction heating thermo-mechanical fatigue (TMF) were performed on Hastelloy X superalloy in the small and large scale yielding in plane stresses mode. The crack growth rates were measured and formulated by fracture mechanics parameters. Furthermore, the fatigue life was predicted by employing resistance curves technique. The TMF behavior of this superalloy was investigated. The results demonstrated that in-phase loading TMF conditions lead to short fatigue life (more crack growth rate) at high strain amplitudes and temperatures up to 600 °C. For higher temperatures, the predominant damage was due to creep. A model based on damage contributions due to pure fatigue and cyclic creep has been presented for predicting TMF crack growth rates. Fracture mechanic method was used to suggest a model for fatigue part of TMF crack growth rate, while the temperature effects during TMF crack growth rate was considered to be due to cyclic creep. In addition the TMF crack healing or crack closure occur during application of induced eddy currents were investigated explicitly, as environmental effects of induction heating. The results show the higher current density in the crack tip area produced more heat and resulted in a significant rise in temperature. So it was concluded that the compressive thermal stress due to change of thermal expansion causes crack healing.

1. Introduction

The gas turbine engine components at high temperatures are exposed to thermo mechanical fatigue (TMF). The Hastelloy X is one of the nickel based super alloys in the hot section parts of engine that possesses an exceptional combination of high-temperature strength, oxidation resistance, fabricability and it has also been found to have exceptionally resistant to stress-corrosion cracking in petrochemical applications [1]. Thermo-mechanical fatigue crack growth is more complicated than pure fatigue crack growth because it includes time dependent material behavior characteristics such as creep and oxidation. According to Antolovich and Saxena [2], TMF, can be viewed as a fatigue damage process under simultaneous changes in temperature and mechanical loads. Some studies have been done on the TMF behavior of nickel based super alloys for fatigue life prediction [3–8]. In most of them, isothermal fatigue (IF), in-phase (IP) and out-of-phase (OP) TMF results have been compared and the strain and damage based approaches were investigated by fracture mechanics parameters such as the stress intensity factor K, the J-integral and the crack-tip opening displacement (CTOD).

Despite the fact that a variety of life prediction models have already been proposed for TMF, environ-mental effects are mostly not explicitly included. Christ [9] illustrated the variety of environmental, oxygen and hydrogen, influences which can take place during thermo mechanical fatigue of metallic engineering materials, and the resulting effects on TMF life.

In the TMF experiments, heating can be accomplished by various techniques including induction, direct resistance, radiant, or forced air heating. Each of these techniques may be considered as environmental effects. In the current study, induction heating has been accomplished and its effect on the TMF behavior has been investigated. It could be considered as AC magnetic field or eddy current can affect on the TMF crack growth rate. It is known that high density electric current field influences on the fatigue crack healing [10]. Restoration of fatigue damage by high density electric current in stainless steel has also been demonstrated [11]. Also one

* Corresponding author.
E-mail addresses: m-esmaeilzadeh@semnan.ac.ir (M. Esmaeilzadeh), qods@semnan.ac.ir (F. Qods), arabi@iust.ac.ir (H. Arabi), bmsadeghi@iust.ac.ir (B.M. Sadeghi).

http://dx.doi.org/10.1016/j.ijfatigue.2016.12.036
0142-1123/

may consider eddy current treatment as a novel and effective method for crack healing. Healing of Fatigue Crack in 1045 Steel has also been investigated by Using Eddy Current Treatment [12]. Crack closure strongly affects the fatigue crack growth rate and thus, the fatigue life of components. Fatigue crack closure under in-phase and out-of-phase thermo mechanical fatigue loading using a temperature dependent strip yield model has been investigated in [13].

In this paper, crack growth rates due to fatigue and induction heating TMF in plates of Hastelloy X superalloy were investigated by fracture mechanic technique. For accomplishing the objectives, room temperature fatigue tests at various stresses were initially applied and then crack growth rates were formulated using stress intensity factor and J-integral parameters. Besides, by extracting the resistance curves, a simple method for prediction of fatigue life has been proposed. The TMF tests in IF, IP and OP were performed in order to investigate TMF behavior of Hastelloy X. In addition, new models for predicting crack growth rate and TMF life on the basis of the amounts of contributions of fatigue and creep on TMF were proposed. Effects of temperature on TMF crack growth rate were considered utilizing fracture mechanic equations. Also fatigue and cyclic creep contributions at various temperatures were presented in a robust mathematical model. Finally, the TMF crack healing and crack closure by induced eddy currents, as environmental effects of induction heating, have been investigated explicitly in this research.

2. Experimental methods

2.1. Material, specimen preparation and apparatuses

The starting material used in this investigation was Hastelloy X, a nickel based superalloy, with a chemical composition, identical to UNS N06002 standard shown in Table 1. It was delivered in the form of plate shape with 2 mm thickness. These plates were heat treated at 1175 °C for 1 h and then rapidly cooled in air.

The compact tension CT specimens, that are single edge-notch specimens loaded in tension, were fabricated with the dimensions given in Fig. 1. It should be mentioned that standard CT specimen, fatigue precracking and other apparatuses such as clevis and pins met the requirements of ASTM E 647 [14]. The specimens with 2 mm thickness then subjected to tensile test in plane stress mode.

In order to measure the crack size and crack opening displacement, COD, an EOS 700D digital camera with 5184 × 3156 pixel resolution and a crack gauge were used. For application of induction heating in thermo mechanical fatigue, TMF, an elliptic coil composed of 7 turns of copper wire was used. The elliptic shape of coil lets to symmetrical heating in two sides of the plate. A power within the range of 1.6–2 kW was used. Water circulation for cooling of copper wires and also grips and fixtures for holding the specimen were used. Fig. 2 shows set up of TMF equipments.

2.2. Experimental procedures

According to fracture mechanics, fatigue crack growth could be investigated by two different scales: linear elastic fracture mechanics (LEFM) and elastic plastic fracture mechanics (EPFM). The ASTM E 647 [14] standard required that the specimen be predominantly elastic at all values of applied force, thus for the CT specimen the following relation is required for LEFM:

$$(\boldsymbol{W}-\boldsymbol{a}) \geqslant (4/\boldsymbol{\pi})(\boldsymbol{K}_{\max}/\boldsymbol{\sigma}_{\boldsymbol{YS}})^{2} \quad (1)$$

where: W is the total ligament length, a is the crack length and $(W–a)$ = the length of specimen's uncracked ligament (see Fig. 1), and $\sigma_{YS} = 0.2\%$ offset yield strength determined at the same temperature that fatigue crack growth rate data were taken. Here K_{max} is the maximum stress intensity factor. For the CT specimen one can calculate ΔK by using the following relationship [14]:

$$\Delta \boldsymbol{K} = \frac{\Delta \boldsymbol{P}}{\boldsymbol{B}\sqrt{\boldsymbol{W}}} \frac{(\mathbf{2}+\boldsymbol{\alpha})}{(\mathbf{1}-\boldsymbol{\alpha})^{\frac{3}{2}}} (\mathbf{0.886}+\mathbf{4.64}\boldsymbol{\alpha}-\mathbf{13.32}\boldsymbol{\alpha}^{2}+\mathbf{14.72}\boldsymbol{\alpha}^{3}-\mathbf{5.6}\boldsymbol{\alpha}^{4}) \quad (2)$$

Table 1
Chemical composition of Hastelloy X in wt%.

Element	Ni	Cr	Fe	Mo	W	Mn	Co	Si	P,S
wt%	47.2	22.8	18.5	8.2	0.71	0.49	0.73	0.24	<0.008

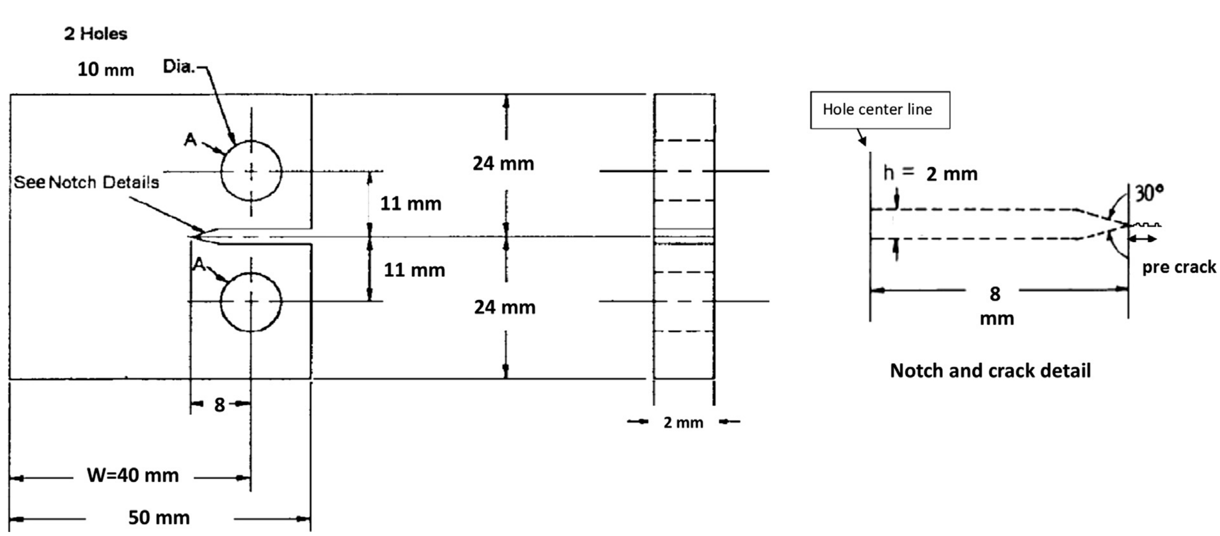

Fig. 1. The compact tension specimen geometry.

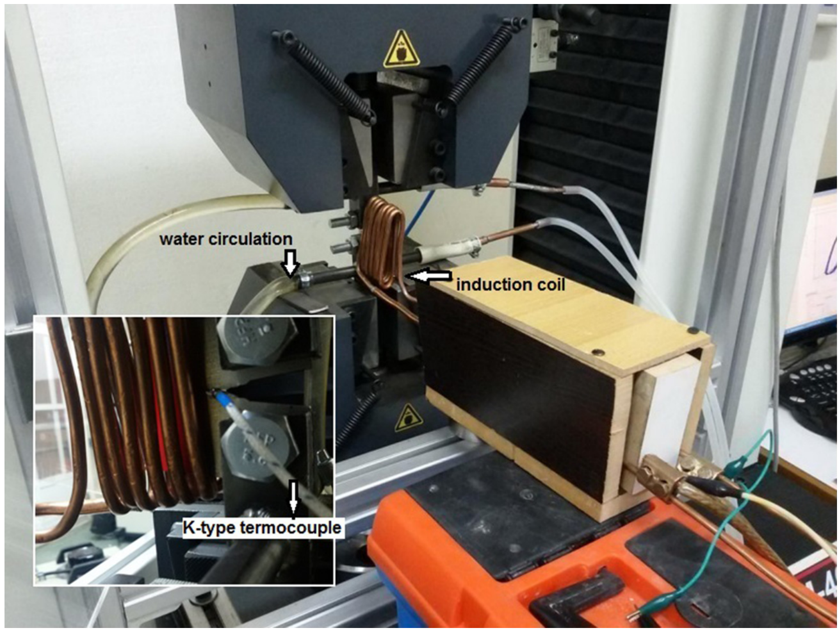

Fig. 2. Set up of TMF equipments.

where: $\alpha = a/W$; expression valid for $a/W \geqslant 0.2$ [14].

For EPFM mode, the specimen's uncracked ligament in CT should be smaller than Eq. (1).

Using Eqs. (1) and (2), forces were determined for LEFM and EPFM modes for each temperature.

Incremental polynomial method as a recommended data reduction technique was used for computing *da/dN* (ASTM E 647-APPENDIX X1). In addition of ΔK and *da/dN*, J-integral was employed for calculating crack growth rate on the basis of energy models specially for EPFM modes. J-integral calculation for CT specimens was done according to ASTM E 1820 [15] as follows:

$$J = J_e + J_p \tag{3}$$

$$J_e = \frac{K^2(1-\nu^2)}{E} \tag{4}$$

$$J_p = \frac{\eta A_{pl}}{B_N b_0} \tag{5}$$

where: A_{pl} is the area under load-displacement, B_N is the net thickness, b_0 = uncracked ligament and $\eta = 2 + 0.522\ b_0/W$.

For operational definition of ΔJ_{total}, integration area during the specific load cycle was used which is shown in Fig. 3 [16].

2.2.1. Fatigue at room temperature

Fatigue tests performed at room temperature in both LEFM and EPFM modes. Table 2 shows the conditions of samples and forces used.

2.2.2. Induction heating TMF

TMF test were performed in both LEFM and EPFM modes. Used TMF cycles at constant temperatures, for in-phase, IP, and out of phase, OP, are shown in Fig. 4. The conditions of these tests are also presented in Table 3.

3. Results and discussion

3.1. Room temperature results

Results of crack growth rates were evaluated separately in LEFM and EPFM modes. Fig. 5 shows the results of crack growth rates versus stress intensity factor in the logarithmic scales. These results were extracted from three samples in LEFM mode and plane

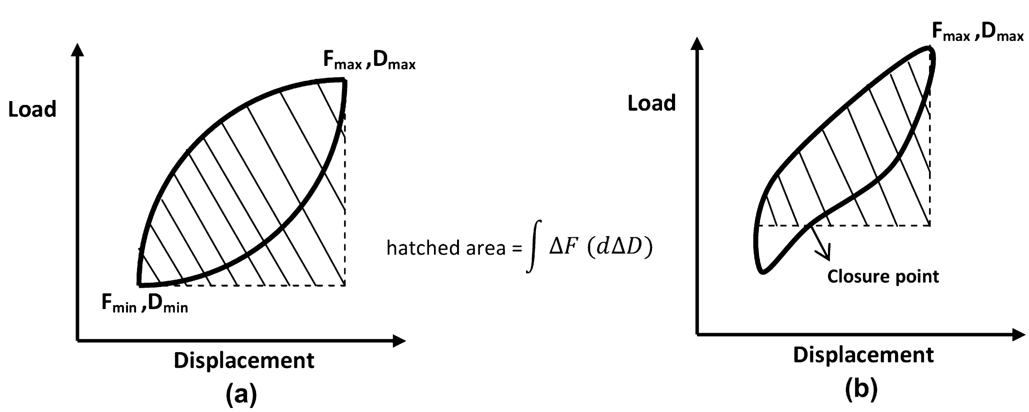

Fig. 3. Load cycle integration area for operational definition of ΔJ_{total}. (a) Without respect to the crack closure level. (b) With respect to the crack closure level [16].

Table 2
Test conditions of CT fatigue samples at room temperature.

a_0 (crack length mm)	F_{max} (N) ~	F_{min}	Fatigue fracture mechanics
10 mm (notch + 2 mm pre crack)	7000	0	EPFM
10 mm (notch + 2 mm pre crack)	8000	0	EPFM
9 mm (notch + 1 mm pre crack)	8000	0	EPFM
14 mm (notch + 6 mm pre crack)	6000	0	EPFM
14 mm (notch + 6 mm pre crack)	4000	0	EPFM
13 mm (notch + 5 mm pre crack)	2300	0	LEFM
15 mm (notch + 7 mm pre crack)	5000	0	EPFM
24 mm (notch + 16 mm pre crack)	1300	0	LEFM
24 mm (notch + 16 mm pre crack)	2300	0	EPFM
27 mm (notch + 19 mm pre crack)	800	0	LEFM
27 mm (notch + 19 mm pre crack)	700	0	LEFM
27 mm (notch + 19 mm pre crack)	600	0	LEFM

stress mode for maximum forces of F_{Max} = 800, 700 and 600 N. m and C, in Paris and Erdogan [18] equation were calculated by the least square analysis for LEFM samples at room temperature as follows:

$$\frac{da}{dN} = 10^{-11.8} \cdot \Delta K^{5.7} \tag{6.a}$$

$$\frac{da}{dN} = 3 * 10^{-7} \cdot \Delta J^{3} \tag{6.b}$$

For investigating EPFM, cyclic loads were used and the results were evaluated for stable and un-stable crack growth. Fig. 6 shows the maximum cyclic loads, i.e. F_{max} = 8000 and 6000 N used in EPFM. The arrows in Fig. 6 show starting of un-stable crack growth. As it mentioned for EPFM for intermediate and large scale forces using J-integral approach was more suitable than stress intensity factor. In the new approach used in this study for fatigue life prediction, J Calculation was initially used for the Resistance Curve of un-stable crack. Then the fatigue life was predicted from these curves.

For the CT specimen at a point corresponding to crack length, a (i), displacement, v(i), and force, P(i), on the graph of specimen load versus displacement, J-integral R-curve was calculated according to technique described in Ref. [15] as follows:

$$J_{(i)} = \frac{K_{(i)}^2(1-\nu^2)}{E} + J_{pl(i)} \tag{7}$$

where: $K_{(i)}$ can be calculated from Eq. (2) and

$$J_{pl(i)} = \left[J_{pl(i-1)} + \left(\frac{\eta_{(i-1)}}{b_{(i-1)}}\right)\frac{A_{pl(i)} - A_{pl(i-1)}}{B}\right] \cdot \left[1 - \gamma_{(i-1)}\frac{a_{(i)} - a_{(i-1)}}{b_{(i-bf1)}}\right] \tag{8}$$

where: $\eta_{(i-1)}$ = 2.0 + 0.522 $b_{(i-1)}$/W, and $\gamma_{(i-1)}$ = 1.0 + 0.76 $b_{(i-1)}$/W.

The quantity $A_{pl(i)} - A_{pl(i-1)}$ in Eq. (8), is the increment of plastic area under the load that is plastic load-line displacement between lines of constant displacement at points (i−1) and i.

J-integral Resistance-curve extracted from un-stable crack part of a sample with a_0 = 9 mm, F_{max} = 8000 N, is shown in Fig. 7. Also Δj-Δa curves for samples in Fig. 6 (EPFM) and a sample in LEFM are compared with the calculated R-curve. At the same temperature, results demonstrate that un-stable crack growth (starting of fatigue failure) occurred when J-integral reach to a critical value on the un-stable crack R-curve. This approach can predict fatigue life in both LEFM and EPFM modes without any extra tests or more information such as ΔK_c. In order to use the mentioned approach for LEFM or EPFM, Δj-Δa curve should be plotted. This is possible

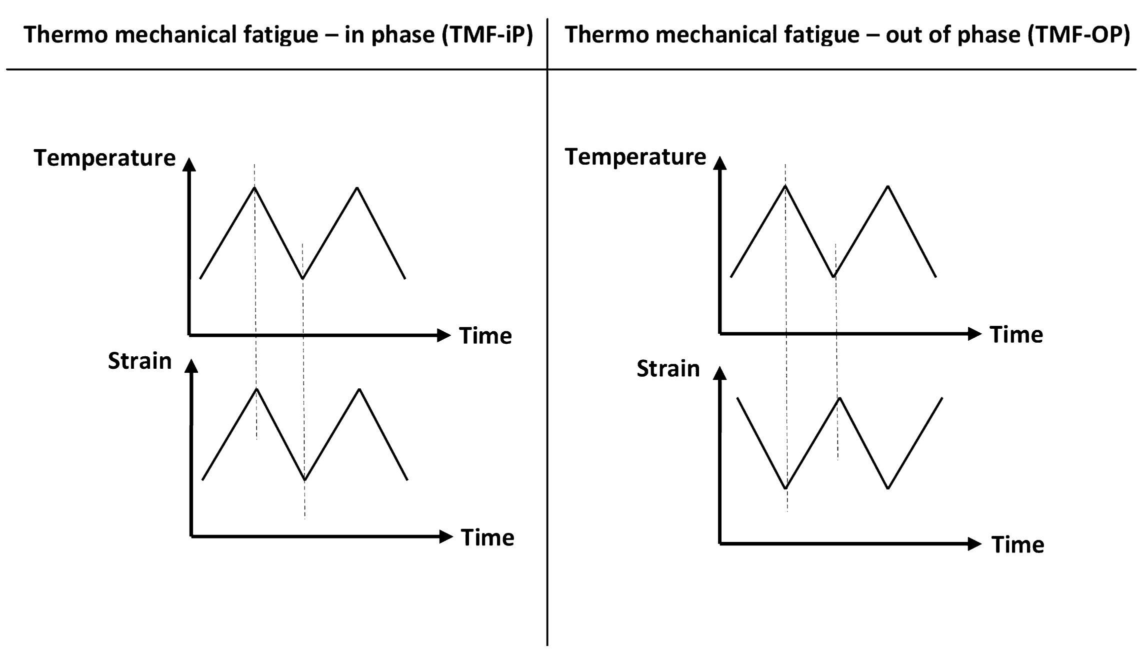

Fig. 4. In - phase and out - of - phase TMF cycles [17].

Table 3
Test conditions of CT -TMF samples at various temperatures.

a_0 (crack length mm)	F_{max} (N) ~	F_{min} (N)	TMF phase	Temperature (°C)	Fatigue fracture mechanics
17	1500	0	T-constant	500	LEFM
17.1	1500	0	IP	80–500	LEFM
	1500	0	IP	415–500	LEFM
	1500	0	IP	250–500	LEFM
17.2	1500	0	OP	500–250	LEFM
17.3	1500	0	IP	600–740	LEFM
17.4	1500	0	OP	740–600	LEFM
17.5	2600	0	T-constant	500	EPFM
17.6	3200	0	T-constant	500	EPFM
19.4	2600	0	IP	415–500	EPFM
	2600	0	IP	370–500	EPFM
19.5	2600	0	OP	500–370	EPFM
20	2600	0	T-constant	740	EPFM

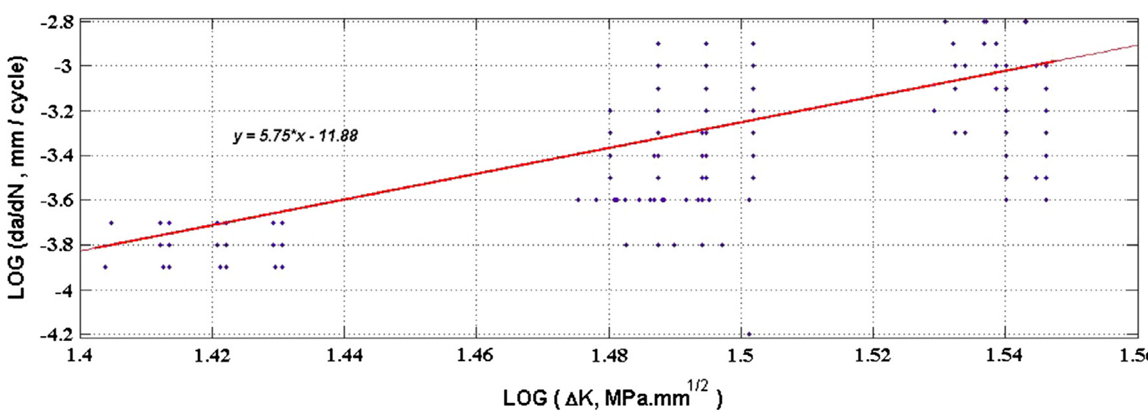

Fig. 5. Log(da/dN) vs Log(ΔK) for Hastelloy X at room temperature and LEFM.

by equating Eq. (6.b) to Eq. (6.a) or Eq. (12) which will be described as an integrated equation. So, by cutting of the mentioned curve with R-curve of un-stable crack, $\Delta j_{critical}$ and $\Delta a_{critical}$ can be extracted. Also increase in Δj in the specified cycles should be clearly established. This information let us to predict the number of cycles lead to fatigue failure. For example, in a LEFM fatigue case for, F_{max} = 2300 N and a_0 = 13 mm, which is shown in Fig. 7, it is possible to calculate the Δj-Δa equation. Following the above mentioned procedure, number of cycles to start the un-stable crack was calculated as follows:

The equation of fatigue case for, F_{max} = 2300 N, a_0 = 13 mm is:

$$\boldsymbol{\Delta j = 0.0054\ \Delta a^4 - 0.1192\ \Delta a^3 + 0.9078\ \Delta a^2 - 0.4323\ \Delta a + 12.92} \quad (9)$$

and un-stable crack R-curve (see Fig. 7) can be determined by:

$$\boldsymbol{\Delta j = -2.1514\ \Delta a^2 + 48.187\ \Delta a + 100.3} \quad (10)$$

By equating Eq. (9) to Eq. (10), $\Delta j_{critical}$ & $\Delta a_{critical}$ were calculated, i.e. $\Delta j_{critical}$ = 231 mj/mm^2 and $\Delta a_{critical}$ = 19.23 mm. The number of cycles to start the un-stable crack, N_f, was calculated as 5274 cycles. The accuracy of the above method was evaluated by experimental validation test which conformed that the actual N_f was 5473 cycles which is in good agreement with the calculated one.

Results obtained for crack growth rate for hastelloy X- CT samples in EPFM, for intermediate and large stresses under plane stress mode could be integrated in one curve. Fig. 8 shows *da/dN* versus total J-integral for all the data presented in Table 2. Eqs. (6.b) and (11) are considered as suitable related equations for LEFM and EPFM respectively. The polynominal curve in Fig. 8 shows the best fitting of fatigue results in EPFM (for stable and unstable cracks) at room temperature.

$$\boldsymbol{\frac{da}{dN} = -3 * 10^{-13} \cdot J^5 + 3 * 10^{-10} \cdot J^4 - 1 * 10^{-7} \cdot J^3 + 2 * 10^{-5} \cdot J^2 + 0.00006 \cdot J} \quad (11)$$

The integrated results can be evaluated by stress intensity factor for both LEFM and EPFM. Fig. 9 shows the logarithmic curve of *da/dN* versus ΔK based on the following related equation.

$$\boldsymbol{\frac{da}{dN} = 10^{-9.8456} \cdot \Delta K^{4.3699}} \quad (12)$$

3.2. Results of TMF

TMF tests in LEFM mode was performed on the CT samples at constant temperature, for in phase and out of phase states. It should be noticed that σ_{YS} in Eq. (1) decrease with increasing temperature. In order to meet the requirements of Eq. (1) for satisfying LEFM, σ_{YS} in the maximum temperature during TMF must be used for calculating the maximum force.

TMF results at constant temperature (500 °C, F_{max} = 1500 N) is shown in Fig. 10a. The related Paris-Erdogan equation (Eq. (13)) for LEFM which was extracted by least square analysis is shown in Fig. 10b. The amount of deviation associated with this equation is much more than that of Eq. (12) at room temperature.

$$\boldsymbol{\frac{da}{dN} = 10^{-32.8} \cdot \Delta K^{20.4}} \quad (13)$$

Comparing Eqs. (13) and (12), it is clear that for the same ΔK, crack growth rate at 500 °C is more than that of room temperature.

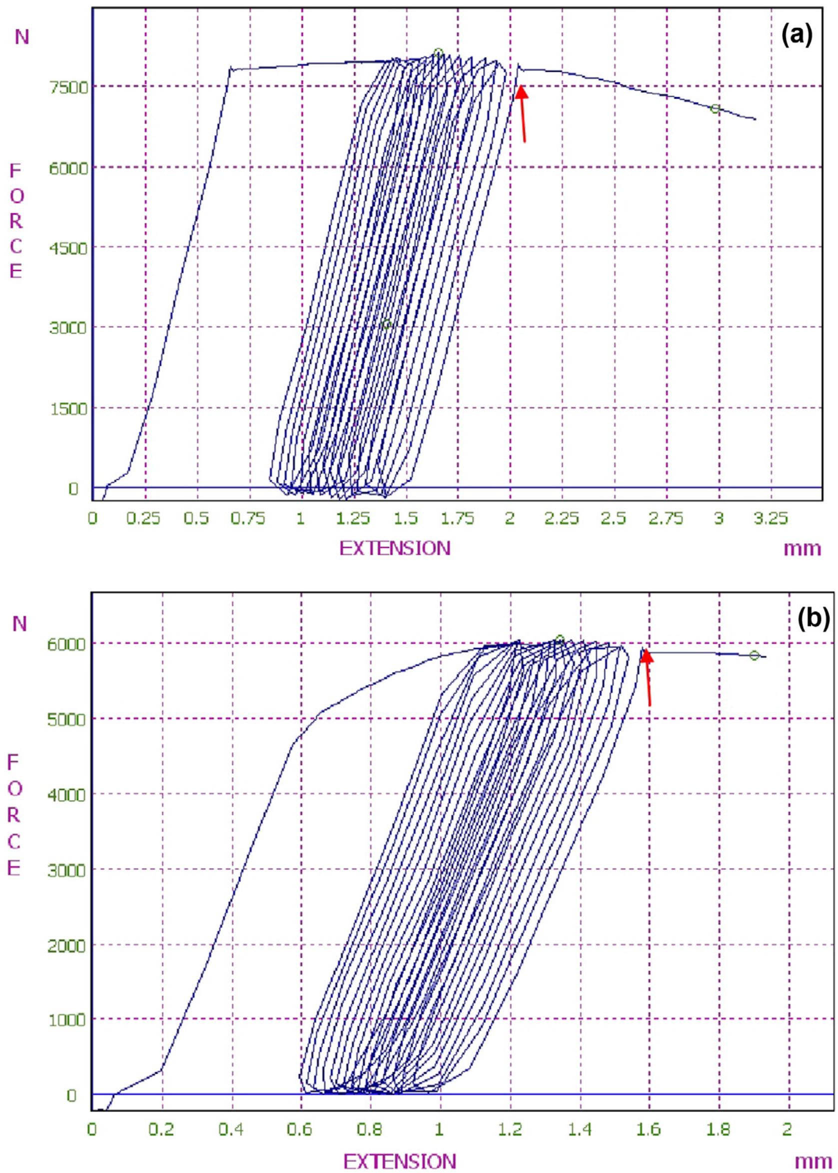

Fig. 6. Cyclic load-displacement curve of CT samples in EPFM-large scale forces: (a) 8000 N, (b) 6000 N.

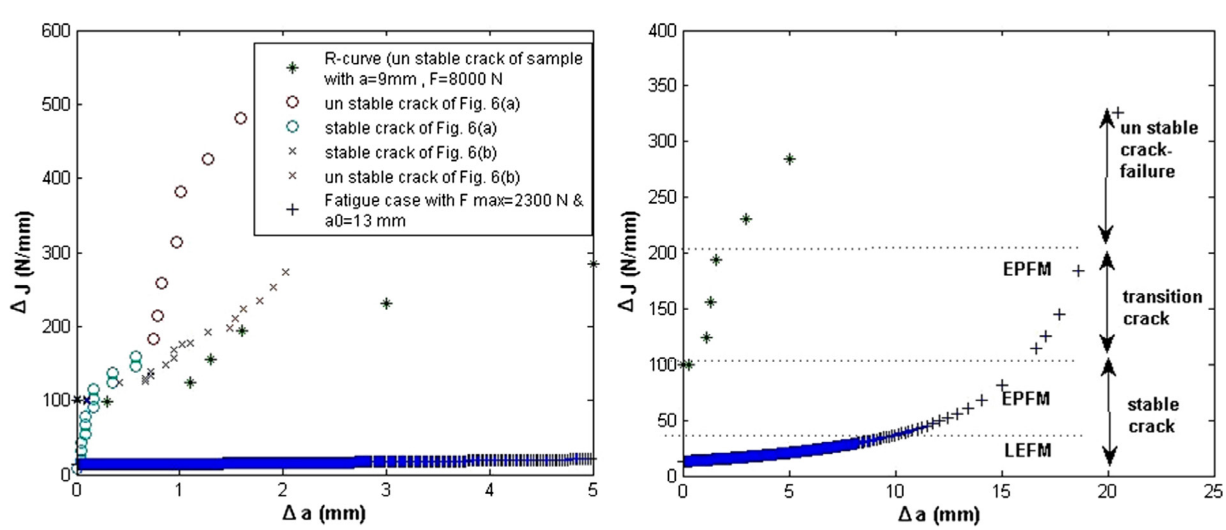

Fig. 7. J-integral resistance curve for un-stable crack and incremental increase in energy during of fatigue in EPFM and LEFM.

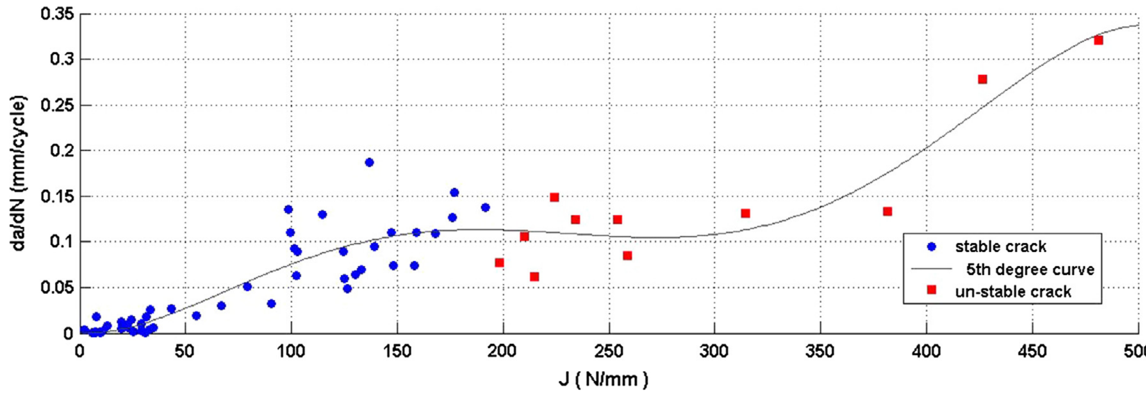

Fig. 8. Integrated results of crack growth rate vs J-integral for LEFM and EPFM.

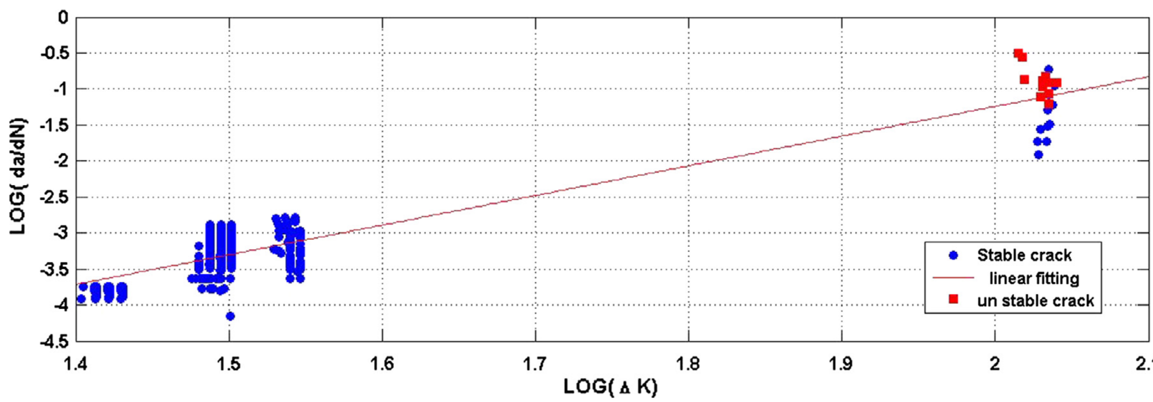

Fig. 9. Integrated results of crack growth rate logarithm vs ΔK logarithm for LEFM and EPFM.

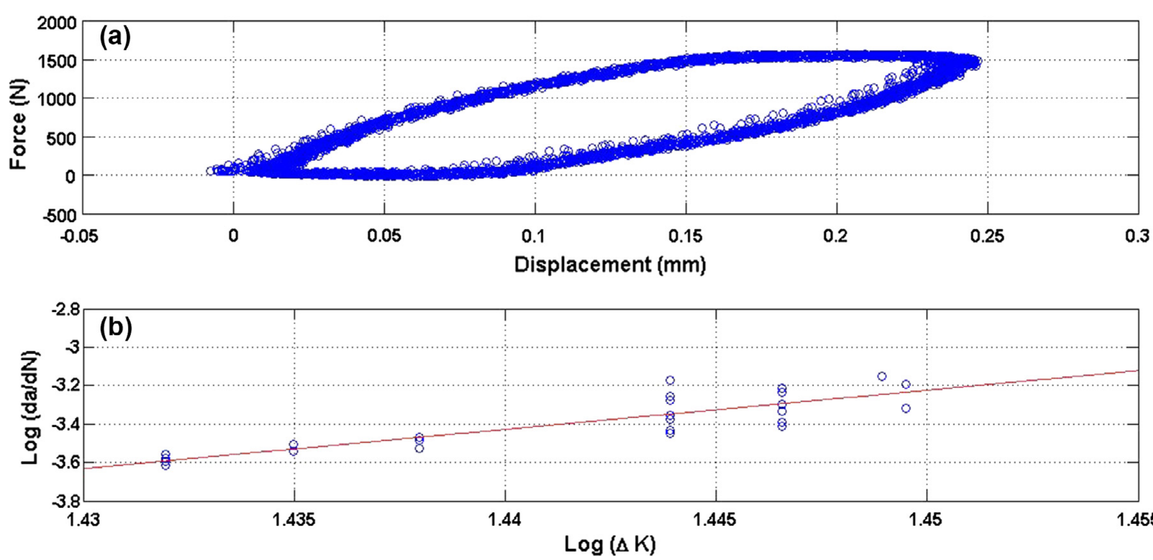

Fig. 10. TMF results at constant temperature (500 °C, F_{max} = 1500 N) for LEFM.

For example if one considers $\Delta K = 28\,\mathrm{MPa}\sqrt{m}$, the crack growth rates at the room temperature and 500 °C become 0.00025 and 0.0005 mm/cycle, respectively.

Results of TMF-IP and TMF-OP in LEFM are shown in Fig. 11. In order to compare of LEFM-TMF results based on energy, total J-integral of TMF and the related crack growth rates are calculated and presented in Table 4. It should be noticed that the total J-integral cannot predict crack growth rate and the TMF types (IP & OP), ΔT and T_{max} have significant effects on fatigue life. Thus the instantaneous J-integral at each temperature should be used in the proposed model presented in Section 3.3.

TMF results in EPFM mode for intermediate and large scale stresses were investigated for the CT samples at constant temperature under IP and OP conditions. Fig. 12 shows cyclic

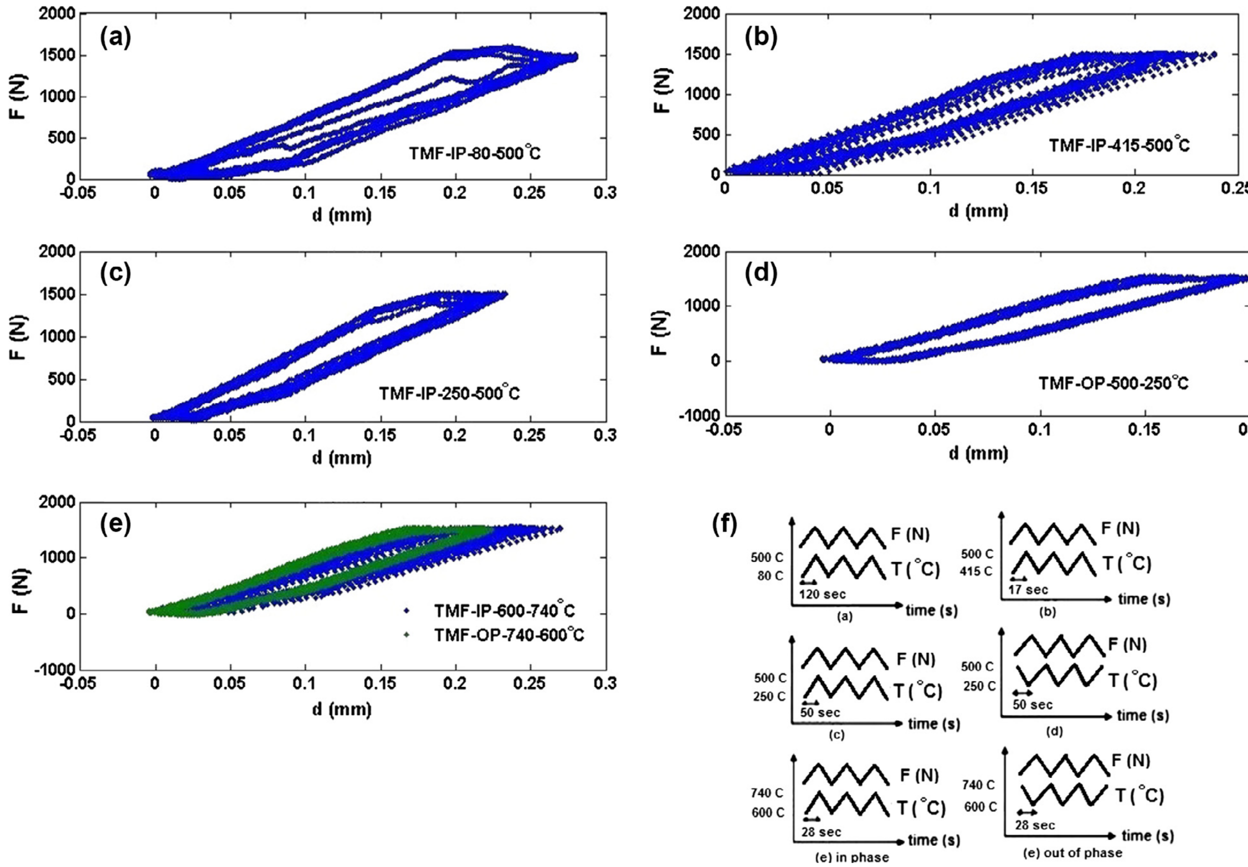

Fig. 11. TMF-LEFM results. (a)–(c) in phase with maximum temperature 500 °C, (d) out of phase with maximum temperature 500 °C, (e) in phase and out of phase with maximum temperature 740 °C and (f) time-Temperature for (a)–(e).

Table 4
Total J-integral for TMF-LEFM results.

TMF conditions	T = 500 C F_{max} = 1500 N	TMF-IP T = 80–500 C F_{max} = 1500 N	TMF-IP T = 415–500 C F_{max} = 1500 N	TMF-IP T = 250–500 C F_{max} = 1500 N	TMF-OP T = 500–250 C F_{max} = 1500 N	TMF-IP T = 600–740 C F_{max} = 1500 N	TMF-OP T = 740–600 C F_{max} = 1500 N
ΔK (MPa$\sqrt{m}$)	28	28	28	28	28	32	32
Total J-integral (mj/mm^2)	10.65	12.1	9.2	10.9	9.4	16	17
Experimental crack growth rate (mm/cycle)	0.0005	0.0004	0.0002	0.0004	0.0004	0.0003	0.0002
Predicted crack growth rate by the proposed model (3.3) (mm/cycle)- without induced eddy current healing	0.00048	0.00041	0.00021	0.00043	0.00047	0.00062	0.00050
Predicted crack healing by induced eddy current (3.4) (mm/cycle)	~0	0.000019	0.000017	0.000025	0.00003	0.00026	0.00027

load–displacement and crack growth rate for intermediate stress for EPFM. Crack growth rate at T = 500 °C (Fig. 12d) was calculated by the following model.

$$\frac{da}{dN} = 10^{-12.5} \cdot \Delta J^{7.2} \tag{14}$$

J-integrals calculated for TMF-EPFM are shown in Table 5. The high values of C and m in Eqs. (13) and (14) is an indication that at high temperatures, the fatigue results for Hastelloy X associated with large amount of error, which shows itself in the form of larger misfit in drawing of da/dN versus ΔJ, see Fig. 12d. When J-integral is used for calculating the crack growth rate, therefore for investigating TMF, one should use another technique.

3.3. Proposed integration model for TMF study

As it mentioned in the previous section application of LEFM or EPFM for investigating under conditions of TMF, in phase and out of phase loading result in different crack growth rate and thus different thermo-mechanical fatigue life based on the crack growth rate will be estimated. Regarding the Classification of the TMF life behavior of engineering materials by Nitta and Kuwabara [19,20], Fig. 13, the TMF behavior of the samples in the current study under in plane stress condition has been classified as Type E′ up to 600 °C for more temperatures, it was classified as Type I.

For using TMF model while considering parameters such as material, loading, geometry and environmental factors, it was

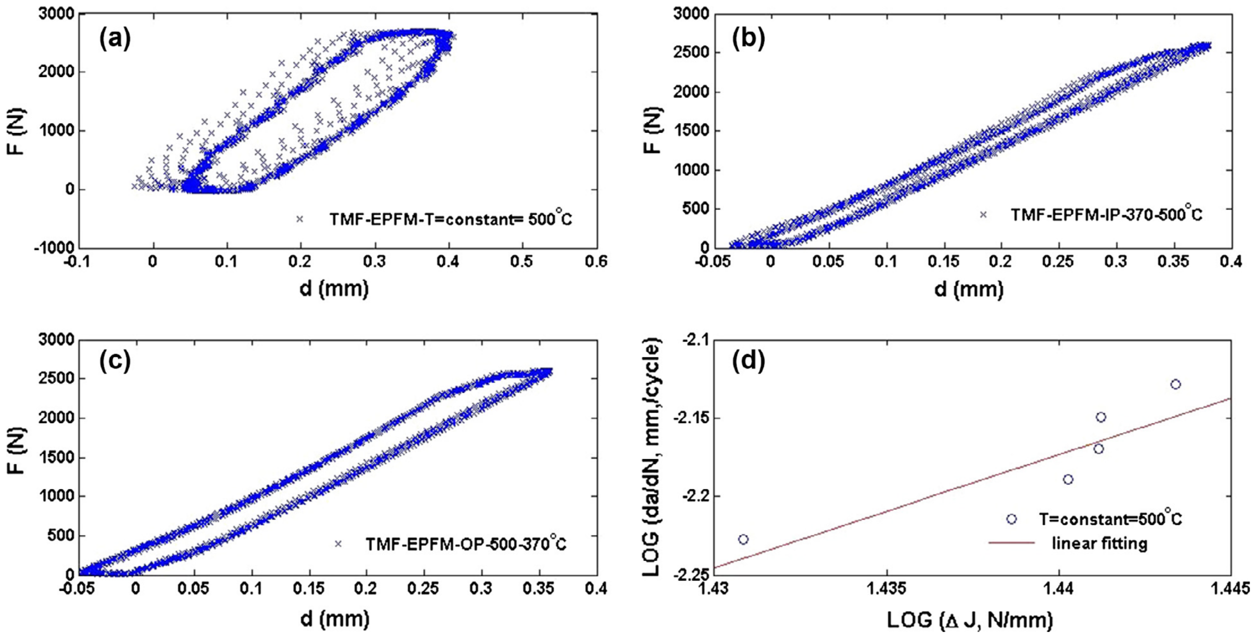

Fig. 12. TMF-EPFM results. (a) constant temperature, (b) in phase, (c) out of phase and (d) logarithmic curve of crack growth rate vs J-integral for T = 500 °C.

Table 5
J-integral calculated for TMF-EPFM results for ΔK = 58 MPa$\sqrt{}$m.

TMF conditions	T = 500 C F_{max} = 2600 N	TMF-IP T = 370–500 C F_{max} = 2600 N	TMF-OP T = 500–370 C F_{max} = 2600 N
J-integral (mj/mm^2)	28.1	28.9	29.8
Experimental crack growth rate (mm/cycle)	0.008	0.0033	0.0025
Predicted rate by the proposed model (mm/cycle), without induced eddy current healing	0.00783	0.00390	0.00323
Predicted crack healing by induced eddy current (mm/cycle)	∼0	0.00051	0.00048

assumed that the overall crack growth rate is due to two sort of contributions, one is owing to pure fatigue and the other due to environmental effects. The environmental effects for the current study are the amounts of temperature (related to creep) and oxidation. For simplicity, a linear superposition law was applied [20]:

$$\frac{da}{dN}(TMF) = \frac{da}{dN}(fatigue) + \frac{da}{dN}(creep) + \frac{da}{dN}(oxidation) \quad (15)$$

Worth mentioning that a Hastelloy X superalloy has outstanding oxidation resistance at temperatures up to 1200 °C. So in this study the samples did not expose to oxidation damages and the last term of Eq. (15) can be ignored. In conventional standard test methods, creep crack growth rates in metals at elevated temperature using CT specimens subjected to static or quasi-static loading conditions, determination of steady-state creep crack growth rate is required. Because of temperature and stress variations of TMF (IP or OP), the conventional ways to calculate the crack growth rate as a result of creep (*da/dt*) cannot be used. Therefore in this study an energy-based approach was used, so that time dependence of the total J-integral for TMF for the same forces and temperatures were related to creep equivalent (C^*) of the material as the following:

$$C^*(t) = \frac{\partial J(TMF)}{\partial t} \quad (16)$$

The Creep equivalent of J-contour integral used in this study to determine the stress and strain rate distribution ahead of a crack in a component deformed by creep [21]. The $C^*(t)$ for a two-dimensional crack, in the x-z plane with the crack front parallel to the z-axis, is the line integral as presented in the following model [22].

$$C^*(t) = \int_\Gamma \left(W^*(t)dy - T \cdot \frac{\partial \dot{u}}{\partial x} ds \right) \quad (17)$$

where: $W^*(t)$ is instantaneous stress-power or energy rate per unit volume, Γ is path of the integral, that encloses the crack tip, ds is increment in the contour path, T is outward traction vector on ds, $\dot{u}$ is displacement rate vector at ds, $T.\ (\partial\dot{u}/\partial x){\cdot}ds$ is the rate of stress-power input into the area enclosed by Γ.

The magnitude of the $C^*(t)$-integral for the CT specimen at each point can be determined according to the following equation [21,22].

$$C^*(t) = \frac{P\dot{V}_c}{B(W-a)} \frac{n}{n+1} \left(2 + 0.522 \frac{W-a}{W} \right) \quad (18)$$

where, n is creep exponent in the relationship between minimum creep rate and applied stress. The value of n may be obtained from creep test data. If creep tests cannot be performed, the accepted value of n from the literature may be used provided it is for the same type of materials [22]. $\dot{V}_c$ can be calculated by the following equations [23,24].

$$\dot{V}_c = \dot{V} - \frac{\dot{a}B}{P} \left[\frac{2K^2}{E'} \right] \quad (19)$$

where: $\dot{V}$ is load-line displacement rate, a° is crack growth rate, da/dt, P is applied force, $E' = E/(1-\upsilon^2)$ for plane strain and E for plane stress, B is net section thickness and K is stress intensity factor.

TMF type		Dominant damage mode
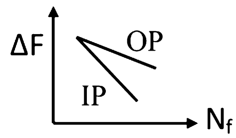	**Type I** **IP loading led to earlier failure**	**creep**
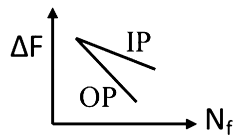	**Type O** **OP loading led to earlier failure**	**Environmental effects**
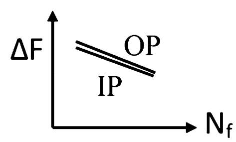	**Type E** **IP & OP loading show nearly effects on fatigue life**	**Neither creep, Nor environmental damage dominate**
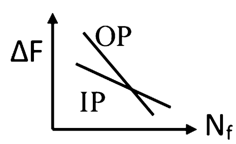	**Type E'** **IP loading at high force amplitude led to earlier failure**	**Creep only on high force amplitudes**

Fig. 13. Classification of the TMF life behavior of engineering materials after Nitta and Kuwabara [19,20].

Replacing $\dot{V}_c$ from Eq. (19) in Eq. (18), creep crack growth rate can be calculated.

$$\dot{\boldsymbol{a}} = \frac{\boldsymbol{E}'}{\boldsymbol{B}\cdot 2\cdot \boldsymbol{K}^2}\left[\boldsymbol{P}\dot{\boldsymbol{V}} - \frac{\boldsymbol{C}^*\cdot(\boldsymbol{n}+\mathbf{1})}{\boldsymbol{n}\cdot\boldsymbol{Y}}\right] \tag{20}$$

where $Y = (1/B\cdot(W\text{-}a))\cdot(2 + 0.522(W\text{-}a)/W)$.

According to Eq. (20), the creep crack growth rate is related to some parameters which they are themselves depended to temperature. Therefore because of temperature variation in TMF; $\dot{\boldsymbol{a}}$ can be calculated by the following relationship.

$$\dot{\boldsymbol{a}}\ \textbf{\textit{creep in TMF}}\left(\frac{\boldsymbol{mm}}{\boldsymbol{cycle}}\right) = \int_{T1\ \ at\ \ P1}^{T2\ \ at\ \ P2} \dot{\boldsymbol{a}}_{creep}(\boldsymbol{T}).\boldsymbol{m}_c\cdot\boldsymbol{dT} \tag{21}$$

where $m_c = dt/dT$, t is time in hour. For a TMF cycle with linear changing in temperature, m_c is equal to $(t_2\text{-}t_1)/(T_2\text{-}T_1)$.

Eq. (21) defines the cyclic creep crack growth rate for TMF tests proposed in this study. For Hastelloy X super alloy as a creep resistance material, the magnitude of C^* (by Eq. (16)) and $\dot{V}$ at TMF testing temperatures have very small values and measurement of these factors requires hundred hours of precision testing. So in this study a combination of NSW model [25,21] for creep crack growth rate which is a function of C^* and strip yield model [26] was used to estimate crack growth rate as the following:

$$\dot{\boldsymbol{a}}_{creep}(\boldsymbol{T}) = \frac{(\boldsymbol{n}+1)\boldsymbol{A}}{\varepsilon_f^*}\left(\frac{\boldsymbol{C}^*}{\boldsymbol{I}_N\boldsymbol{G}\boldsymbol{A}}\right)^{\frac{n}{n+1}}\cdot \boldsymbol{r}_c^{\frac{1}{n+1}} \tag{22}$$

where A is the coefficient from the secondary creep power law, G is the shear modulus, r_c is the radius of the creep plastic zone (assumed to be equal to ρ, the plastic zone size calculated by Dugdale strip yield model [27], and is equal to $\rho = \pi K^2/8\cdot\sigma_0^2$), $\boldsymbol{\varepsilon}_f^*$ is the creep ductility ($\boldsymbol{\varepsilon}_f^* = \boldsymbol{\varepsilon}_f$ for plane stress and $\varepsilon_f^* = \varepsilon_f/50$ for plane strain) and I_N is a non-dimensional function of the plastic strain hardening exponent N. I_N was determined numerically in [28] as the following:

$$\boldsymbol{I}_N = \mathbf{7.2}\left(\mathbf{0.12} + \frac{\mathbf{1}}{\boldsymbol{N}}\right)^{\mathbf{0.5}} - \frac{\mathbf{2.9}}{\boldsymbol{N}}\ \textbf{\textit{for plane stress}} \tag{23.a}$$

$$\boldsymbol{I}_N = \mathbf{10.3}\left(\mathbf{0.13} + \frac{\mathbf{1}}{\boldsymbol{N}}\right)^{\mathbf{0.5}} - \frac{\mathbf{4.6}}{\boldsymbol{N}}\ \textbf{\textit{for plane strain}} \tag{23.b}$$

Also $\dot{V}_c$ is approximated by $\dot{V}_c \approx \dot{\varepsilon}_s = A\left(\frac{\sigma}{G}\right)^n$ [26] and C^* could be calculated by Eq. (18).

For the current study, the relation of the mentioned material properties, E, n and N, to temperature were obtained from [1,29] and the results are given in Table 6.

The new proposed model in the current study, for calculation of the pure fatigue crack growth rate at various temperature, is in fact an energy based equation at room temperature (e.g. Eqs. (6.b) and (11)) which can be used in association with yield stress and the crack tip opening displacement at any temperature which TMF test is performed. The relationship between J and CTOD has been established by Shih [30] as the following:

Table 6
Relationship of the required parameters for calculation of the creep crack growth rate, with temperature for Hastelloy X.

E (Gpa) –T (°C)	n-T (°C)	N- T (°C)
E = –0.0658 T + 210.39	n = –3E–08 T^3 + 4E–05 T^2 – 0.0002T	N = –7E–10T^3 + 6E–07T^2 + 1E–05T + 0.1502

$$\boldsymbol{CTOD} = \boldsymbol{d_n}\frac{\boldsymbol{J}}{\boldsymbol{\sigma_0}} \tag{24}$$

where d_n is a dimensionless constant given in [16] and ASTM E 1820-11, the value of the dn depends on the hardening behavior of the material. For this study, it was found that Eq. (24) follows the dugdale model [27] for strip yield model and so d_n is equal to one. The load- line displacement, V, for CT samples can be given by the following equation [15].

$$\boldsymbol{CTOD} = \delta_{(\boldsymbol{i})} = \frac{\boldsymbol{K}^2_{(\boldsymbol{i})}}{2\boldsymbol{\sigma_{YS}E}} + \frac{[\boldsymbol{r_p}(\boldsymbol{w}-\boldsymbol{a_0})]\boldsymbol{Vpl}}{[\boldsymbol{r_p}(\boldsymbol{W}-\boldsymbol{a_0})+\boldsymbol{a_0}]+\boldsymbol{z}} \tag{25}$$

where r_p is the plastic rotation factor, its values have been given in Ref. [15]. r_p is consider to be 0.521 and z is equal to 10 mm for the current study of TMF tests.

Combining Eqs. (25) and (24) and inserting the value of $J(\sigma_{0,}V_{pl,fatigue})$ in the Eqs. (6.b) and (11), the pure fatigue equation for crack growth rate, $\dot{a}_{fatigue}$ $(\sigma_{0,}V_{pl,fatigue})$ can be calculated for each temperature. Because of temperature variation in TMF, $\dot{\mathbf{a}}_{fatigue}$ can be calculated by the following relationship.

$$\dot{\boldsymbol{a}}\ \boldsymbol{fatigue\ in\ TMF}\left(\frac{\boldsymbol{mm}}{\boldsymbol{cycle}}\right) = \int_{\boldsymbol{T1atp1}}^{\boldsymbol{T2atp2}} \boldsymbol{f}(\boldsymbol{T})\cdot\boldsymbol{m_f}\cdot\boldsymbol{dT} \tag{26}$$

where $f(T)$ is the modified pure fatigue crack growth rate (mm/cycle) for TMF which is calculated by substitution of J $(\sigma_0(T),$ $V_{pl,\ fatigue}$ $(T))$ in the room temperature equation (e.g. Eqs. (6.b) and (11)) and $m_f = dN/dT$ which is equal to $1/(T_2-T_1)$ for a TMF cycle having a linear change in temperature.

It should be mentioned that for Hastelloy X super alloy, the creep crack growth rate has very small value in comparison with that of fatigue, up to 600 °C. Therefore creep crack growth could be ignored for temperatures up to 600 °C and as a result creep/fatigue interaction was considered as negligible in this research. The relationship between the yield stress and temperature obtained from [29] for Hastelloy X and also the relation between V and temperature was extracted for each experimental TMF tests and used to calculate the pure fatigue crack growth rate. For calculating various parameters of the proposed model, MAPLE 15 was used [31].

R-curves for TMF under large scale stress where drawn for two temperatures. Fig. 14 shows the R-curves of un-stable cracks at 500 and 740 °C. Then, using the results of TMF-J integral versus Δa and cutting of the TMF-R-curve of un-stable crack, $\Delta J_{critical}$ and $\Delta a_{critical}$ for TMF tests were extracted and used for the TMF life prediction.

It is said [32] that creep/fatigue interaction can produce a complex process of damage, involving fatigue and creep damages due to cyclic stress at high temperature. Also Tang proposed a dual

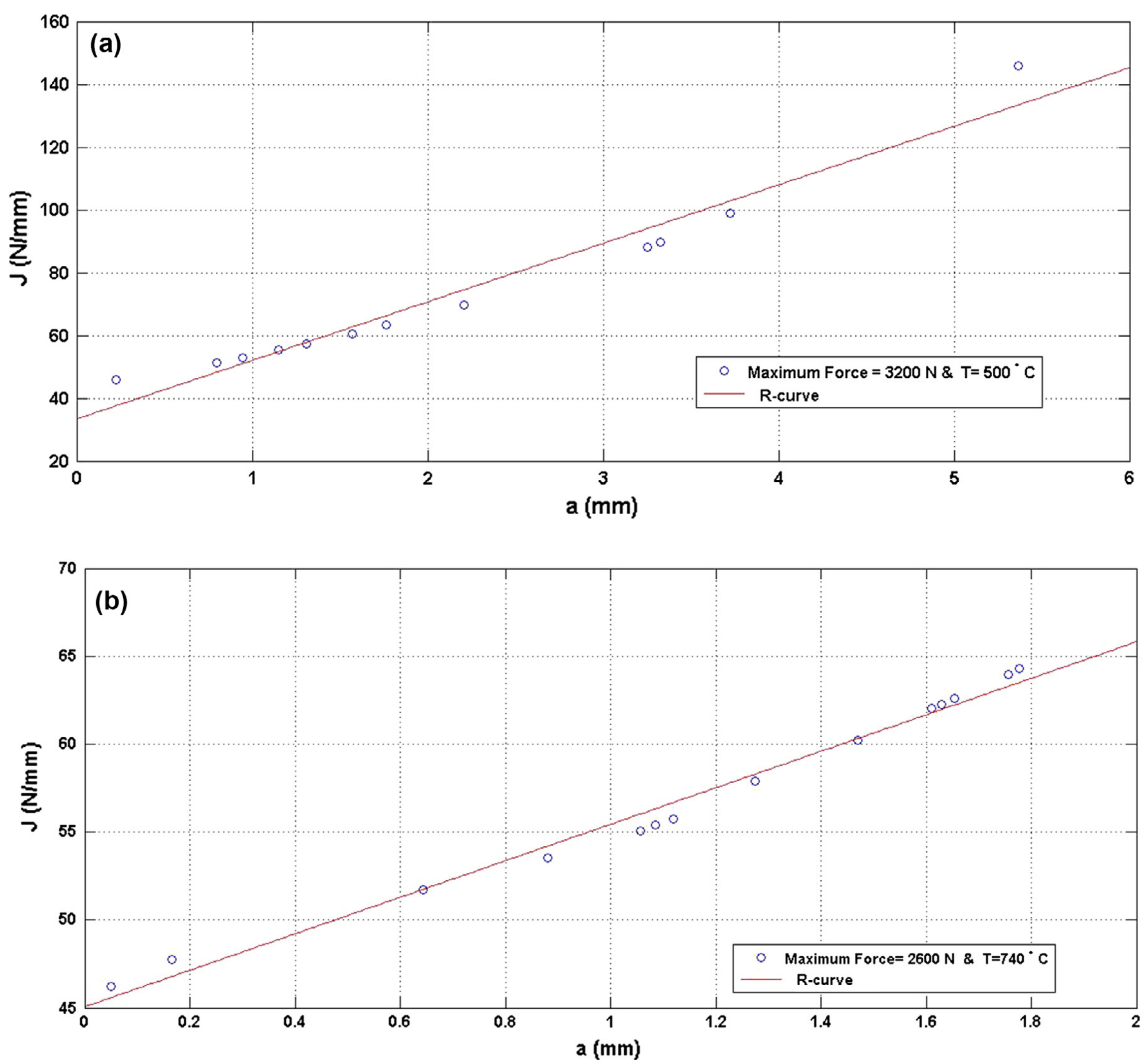

Fig. 14. J-integral Resistance curve for un-stable crack of TMF at (a) 500 °C, (b) 740 °C.

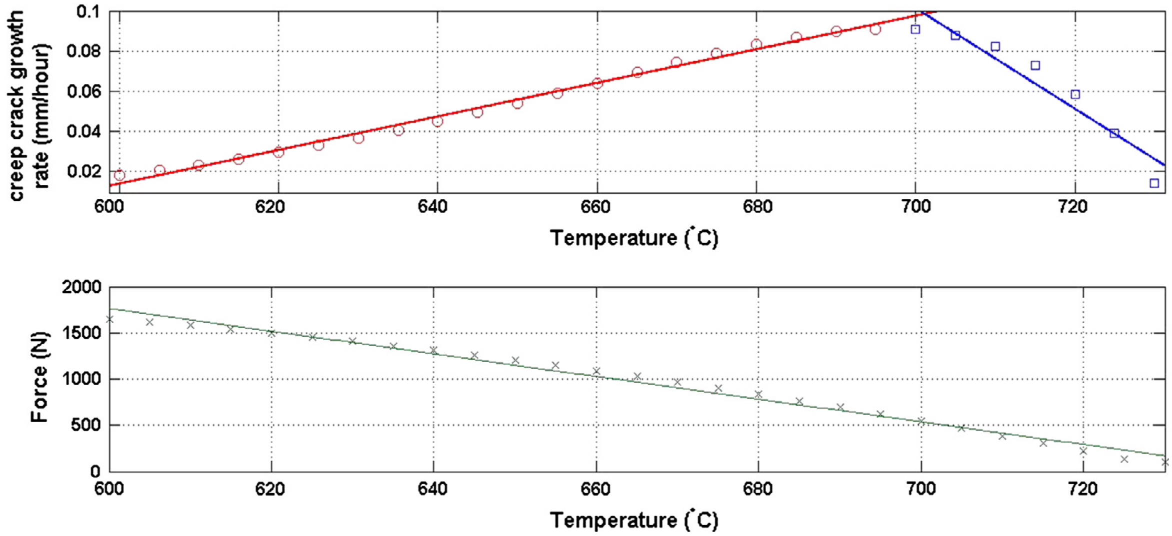

Fig. 15. Cyclic creep crack growth rate for TMF-OP with T = 600–740 °C.

scale fatigue crack growth model [33] to analyze the thermal–mechanical effects in materials under effects of creep and cyclic loading. In the current study, interaction between creep and fatigue was observed for temperatures between 600 °C and 740 °C for TMF-OP which was shown in Fig. 15. This figures shows crack growth rate increased with decreasing force from 1652 N to 620 N and increasing temperature from 600 °C to 695 °C linearly. This indicates that the combined effect of force (which its reduction should reduces crack growth rate) and temperature (which by its increase, the flow of materials would increase caused an increase in the crack growth rate. In the other words, the interaction between the generated dislocations with those already existed within the material, as well as the interaction between the dislocation and the precipitates can cause localized strengthening of the material, hence increased in the crack growth rate was much further than the amount of reduction in growth rate due to force reduction) up to 695 °C. With further increase of temperature to 740 °C and decrease in force to about 100 N the rate of crack growth sharply decreased. This can be due to further softening of the material due to release of dislocations from barriers which helped the material to flow rather than helping the growth of the crack.

A major part of the creep/fatigue interaction which was considered in the cyclic creep part of the proposed model was explained in Eqs. (18)–(23). Certainly other factors such as precipitates can affect the crack growth rate which was not considered in this research.

It should be noted that the proposed model for TMF was based on damage mechanisms contributions for fatigue and creep. Thus the linear superposition law, Eq. (15), considers the accumulation of damages due to plastic strains on the crack tip for the fatigue part and time dependent damages such as micro void accumulation for the creep part. The fatigue crack growth part, $da/dN_{fatigue}$ was modeled for cyclic temperatures and the creep crack growth part, da/dN_{creep}, was modeled for the cyclic stresses, and the interactions of the fatigue/creep are considered separately in Eq. (15).

Comparing the actual experimental data with data obtained from the proposed model (see Tables 4 and 5), it was demonstrated that the actual crack growth rates are less than those predicted by the proposed model. Also the low values of experimental crack growth rates at TMF-IP & OP at max temperature 740 °C, even in the presence of creep, shows the effect of another important parameter which is named as induced eddy current healing in this study. This parameter will be discussed in the following section.

3.4. TMF crack growth healing by induced eddy current

For investigating crack healing-crack closure during induction heating, the mechanism of electromagnetic induction heating was evaluated. For calculating an electromagnetic field it is necessary to solve Maxwell's equations as it has been indicated in [34–36]. This procedure is as follow:

$$\nabla \times \boldsymbol{B} = \boldsymbol{\mu J} \quad (\textit{Ampere's law}) \tag{27}$$

$$\nabla \times \boldsymbol{E} = -\frac{\partial \boldsymbol{B}}{\partial \boldsymbol{t}} \quad (\textit{Faraday's law}) \tag{28}$$

$$\boldsymbol{j} = \boldsymbol{\sigma E} \quad (\textit{Ohm's law}) \tag{29}$$

where E is the electric field intensity, B is the magnetic flux density, J is the current density, μ is the magnetic permeability and σ is the electrical conductivity of the medium.

From the Maxwell's Equation: div $B = 0$. In the scalar field, φ could be defined by a two dimensional vector curling operator as [37,38];

$$\boldsymbol{B} = \boldsymbol{curl}\ \boldsymbol{\varphi} = \nabla \times \boldsymbol{\varphi} = \left(\frac{\partial \boldsymbol{\varphi}}{\partial \boldsymbol{x}2}, -\frac{\partial \boldsymbol{\varphi}}{\partial \boldsymbol{x}1}\right) \tag{30}$$

$$-\boldsymbol{div}\left(\frac{1}{\boldsymbol{\mu}}\nabla\boldsymbol{\varphi}\right) = \boldsymbol{curl}\left(\frac{1}{\boldsymbol{\mu}}\boldsymbol{curl}\ \boldsymbol{\varphi}\right) = \boldsymbol{j} \tag{31}$$

After calculating the induced eddy current density by Eqs. (27)–(31), the thermal problem should be solved in the temperature field resulting from the joule heat according to [38]:

$$\boldsymbol{C}(\boldsymbol{T})\frac{\partial \boldsymbol{T}}{\partial \boldsymbol{t}} - \boldsymbol{div}(\lambda(\boldsymbol{T})\nabla\boldsymbol{T}) = \boldsymbol{P} \tag{32}$$

$$\boldsymbol{P}(\boldsymbol{x},\ \boldsymbol{t}) = \frac{(\boldsymbol{j}(\boldsymbol{x})\boldsymbol{e}^{\boldsymbol{i\omega t}})^2}{\boldsymbol{\sigma}(\boldsymbol{T}(\boldsymbol{x},\ \boldsymbol{t}))} \tag{33}$$

where C is the specific heat, λ is the thermal conductivity and P is the Joule power.

The final model consists of induced eddy currents and temperature distribution which can be solved by Eqs. (27)–(33). It has been demonstrated [12] that the eddy current flows around the crack tip; it accumulates in the crack tip area, leading to much higher current density in the crack tips than in other places in the vicinity of the crack. The higher current density produces more

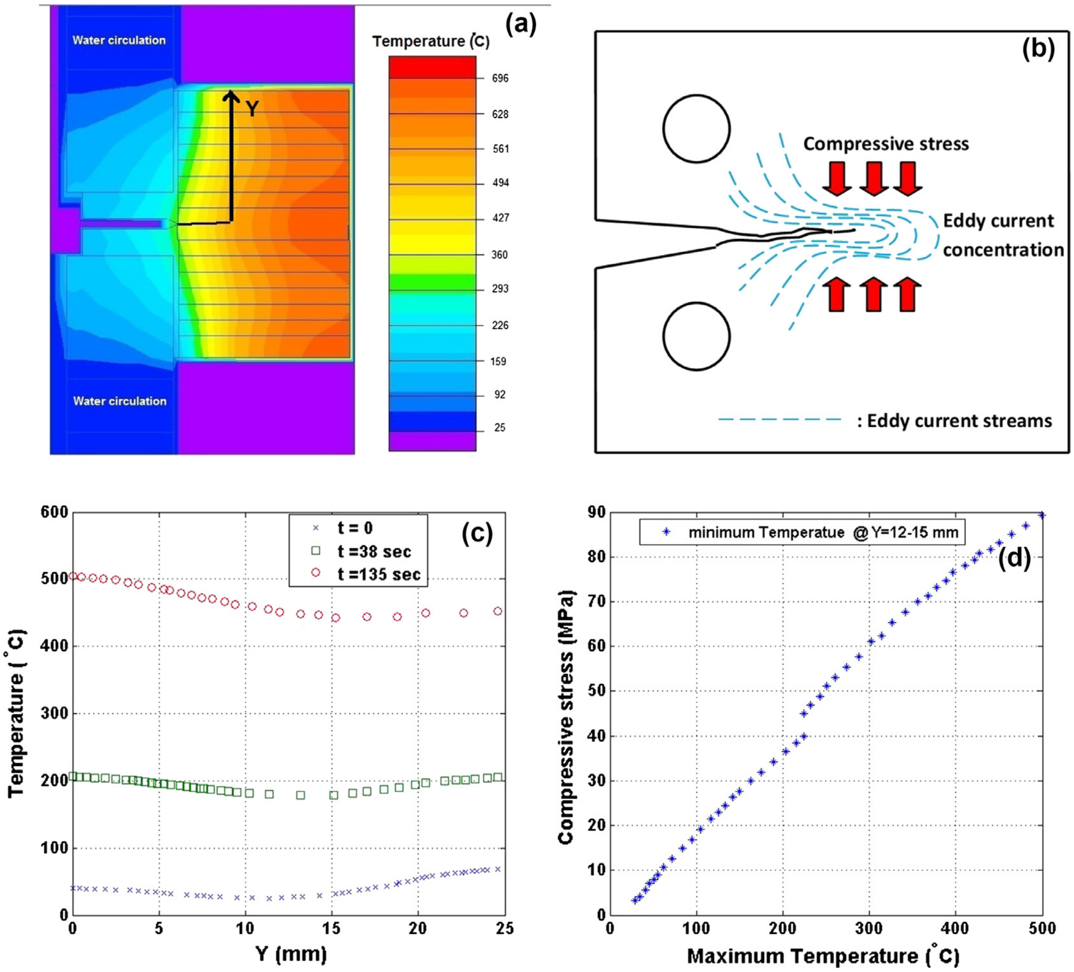

Fig. 16. (a) Temperature distribution, (b) eddy current streams and compressive stress on the crack tip [12] with 17 mm length, (c) temperature gradient on the crack tip at three induction times and (d) compressive stress on the crack tip versus maximum temperature.

heat that results in a significant rise in temperature. Since the thermal expansion rate of metalic material is proportional to the temperature, the thermal expansion in the vicinity of the crack tip will be much more than the thermal expansion in areas far from the crack tip, thus the thermal expansion of the crack tip will be suppressed by the surrounding area. Therefore, there is thermal stress around the crack tip due to the compressive force which is exerted by the surrounding area [12].

The theoretical compressive thermal stress due to change of temperature rise and thermal expansion can be calculated by Hooke's law:

$$\boldsymbol{\sigma} = \boldsymbol{E}(\boldsymbol{T}) \cdot \boldsymbol{\alpha}(\boldsymbol{T}) \cdot \boldsymbol{\Delta T} \tag{34}$$

where α is the thermal expansion coefficient of the specimen and ΔT is the temperature difference between the crack tip area and the neighboring area of the fatigue crack.

Fig. 16 shows the eddy current density, temperature distribution and compressive stress in the crack tip for induction heating TMF tests. The Quick field software according to Ref. [39] can be used for simulation of induction heating based on the Eqs. (27)–(33). The results were validated by experimental measurement of temperatures by K-type thermocouple and also IR-temperature measurements. The compressive stresses led to decrease in crack growth rate and so it plays a role as a crack closure effect and so the Eq. (15) should be modified as the following:

$$\frac{\boldsymbol{da}}{\boldsymbol{dN}}(\boldsymbol{TMF}) = \frac{\boldsymbol{da}}{\boldsymbol{dN}}(\boldsymbol{fatigue}) + \frac{\boldsymbol{da}}{\boldsymbol{dN}}(\boldsymbol{creep}) + \frac{\boldsymbol{da}}{\boldsymbol{dN}}(\boldsymbol{oxidation}) - \frac{\boldsymbol{da}}{\boldsymbol{dN}}(\boldsymbol{eddy\ current\ healing}) \tag{35}$$

It should be mentioned that the compressive stresses have different effects on the pure fatigue and creep contributions. For calculation of the last terms in the Eq. (35), the effects of compressive stresses on fatigue and creep should be measured by Eqs. (24)–(26). By substituting the compressive stresses in Eq. (24) at each temperature one can measures the effect of stress on fatigue. For creep, Eqs. (21)–(23) should be used by substituting the compressive stress in the relationship between $\dot{V}_c$ and stress, i.e. $\dot{V}_c \approx \dot{\varepsilon}_s = A\left(\frac{\sigma}{G}\right)^n$.

The predicted crack healing by induced eddy currents were calculated by the above approach and the results are given in Tables 4 and 5. For this research, maximum healing effects was found to be due to creep contribution of the TMF-LEFM with maximum temperature 740 °C.

The robustness of the presented model was checked. For this purpose contribution of fatigue and creep on crack growth rate model were calculated by MAPLE software [31]. However the effect of induction heating on crack growth model was established by FEM analysis using Quick field software [39]. The root relative squared error between the calculated crack growth rates obtained via Eqs. (15)–(26) and those obtained experimentally were determined by Eq. (36) below. When n is the number of TMF tests.

$$\%\boldsymbol{RRSE} = \sqrt{\frac{\sum_n \left[\left(\frac{da}{dN}(\boldsymbol{experimental\ TMF})\right) - \left(\frac{da}{dN}(\boldsymbol{calculated\ TMF\ by\ model}) - \frac{da}{dN}(\boldsymbol{crack\ healing})\right)\right]^2}{\sum_n \left[\left(\frac{da}{dN}(\boldsymbol{experimental\ TMF})\right) - \left(\frac{da}{dN}(\boldsymbol{average\ of\ experimental\ TMF})\right)\right]^2}} * \mathbf{100} \tag{36}$$

Using the results presented in Tables 4 and 5 and Eq. (36), the mentioned error for n tests was % 4.3, which was included all experimental error sources and uncertainly in the proposed model.

Worth mentioning that the effects of different parameters such as range of temperature, ΔT, range of stress intensity factor, ΔK (includes force and crack length) and maximum temperature of TMF testing on the relative errors of the proposed model were considered and used for error analysis. Results show that most errors of the model are due to TMF-OP which seems to be related to microstructure effects. For some other TMF tests, it was found that a combined parameter such as $\varphi = \frac{\Delta K\cdot(\Delta T+1)}{T_{\max}}$ is a suitable variable to establish a relationship for relative errors (%RE) of the proposed model as follows:

$$\%\boldsymbol{RE} = -\mathbf{0.0186}\boldsymbol{\varphi}^{\mathbf{2}} + \mathbf{0.1564}\boldsymbol{\varphi} + \mathbf{2.0976} \tag{37}$$

As a brief review, the results of this research showed that crack growth on the base of experimental TMF and room temperature fatigue on the Hastelloy X superalloy can be extracted from Eqs. (6), (9)–(11), (13), (14). Also a developed crack growth model was proposed by Eqs. (16), (21), (26) and (35), using the combination of Eqs. (24) and (25) and calculating the crack healing in TMF (by substituting the thermal compressive stress in the related equations of fatigue and creep), this was one of the contributions of this research to the scientific world.

4. Conclusions

Based on the predicted and the experimental results obtained in this research for crack growth rates, the following conclusions were drawn.

1- By extrapolating the fatigue curve of ΔJ-Δa and cutting off the resistance curve for un-stable crack, $\Delta J_{critical}$ and $\Delta a_{critical}$ were extracted. Thus by this method fatigue life of a material can be predicted at room temperature and also at high temperatures.
2- The TMF behavior of Hastelloy X under plane stress condition classified in Type E′ at temperatures up to 600 °C and for higher temperatures, it could be classified in Type I.
3- The new aspect of the proposed model is the use of room temperature equations for fatigue section of TMF crack growth rate. The temperature effects can be considered by fracture mechanic equations. So the cyclic creep part of TMF was investigated on the base of NSW and yield strip model.
4- This study showed that the TMF crack healing by induced eddy currents can be calculated in the AC magnetic and temperature fields. It was demonstrated that the eddy current flows around the crack tip; it accumulates in the crack tip area, leading to much higher current density in the crack tips than in other areas in the vicinity of the crack. The higher current density produced more heat and resulted to a significant rise in temperature. The compressive thermal stress due to change of thermal expansion resulted to crack healing.

Acknowledgements

We would like to acknowledge Mr. Ghorban Esmaeilzadeh as the electronic engineer for design & manufacturing of the induction heating systems. The authors would also like to thank Dr. E. Bagherpour for review the article and his technical suggestions.

Appendix A. Supplementary material

Supplementary data associated with this article can be found, in the online version, at http://dx.doi.org/10.1016/j.ijfatigue.2016.12.036.

References

[1] Haynes international. HASTELLOY ® X ALLOY Data Sheet; 1997. http://www.haynesintl.com/pdf/h3009.pdf.
[2] Antolovich SD, Saxena A. Thermomechanical fatigue: mechanisms and practical life analysis, failure analysis and prevention. ASM Handbook 2002;11:738–45.
[3] Lee D, Shin I, Kim Y, Koo JM, Seok CS. A study on thermo mechanical fatigue life prediction of Ni-base superalloy. Int J Fatigue 2014;62:62–6.
[4] Pelloux RM, Marchand N. Thermal-mechanical fatigue behavior of nickel-base superalloys. Massachusetts Institute of technology Cambridge. Technical Report 86-C-4; 1986.
[5] Liu F, Ai SH, Wang YC, Zhang H, Wang ZG. Thermal-mechanical fatigue behavior of a cast K417 nickel-based superalloy. Int J Fatigue 2002;24(8):841–6.
[6] Huang ZW, Wang ZG, Zhu SJ, Yuan FH, Wang FG. Thermomechanical fatigue behavior and life prediction of a cast nickel-based superalloy. Mater Sci Eng A 2006;432(1–2):308–16.
[7] Jacobsson L, Persson C, Melin S. Thermo-mechanical fatigue crack propagation experiments in Inconel 718. Int J Fatigue 2009;31(8–9):1318–26.
[8] Storgärds E, Simonsson K, Sjöström S, Moverare J. Thermo-mechanical fatigue crack growth modelling in a Ni-based superalloy subjected to sustained load. J Eng Gas Turbines Power 2015;138:1–10.
[9] Christ H-J. Effect of environment on thermomechanical fatigue life. Mater Sci Eng A 2007;468–470:98–108.
[10] Hosoi A, Nagahama T, Ju Y. Fatigue crack healing by a controlled high density electric current field. Mater Sci Eng A 2012;533:38–42.
[11] Tang Y, Hosoi A, Morita Y, Ju Y. Restoration of fatigue damage in stainless steel by high-density electric current. Int J Fatigue 2013;56:69–74.
[12] Yang Chuan, Xu Wenchen, Guo Bin, Shan Debin, Zhang Jian. Healing of fatigue crack in 1045 steel by using eddy current treatment. Materials 2016;9:641. doi: http://dx.doi.org/10.3390/ma9080641. URL: http://www.mdpi.com/1996-1944/9/8/64.
[13] Fischer C, Schweizer C, Seifert T. Assessment of fatigue crack closure under in-phase and out-of-phase thermomechanical fatigue loading using a temperature dependent strip yield model. Int J Fatigue 2015;78:22–30.
[14] ASTM E647. Standard test method for measurement of fatigue crack growth rates. Standardization, vol. 3; 1999.
[15] ASTM E1820. Measurement of fracture toughness 1. Current, vol. 3; 2001 (August), p. 8–9.
[16] Anderson TL. Fracture mechanics: fundamentals and applications. CRC Press; 2005. Jun 24.
[17] Zhuang W, Swansson N. Thermo-mechanical fatigue life prediction: a critical review. DSTO Aeronaut Marit Res Lab, 34; 1998. http://oai.dtic.mil/oai/oai?verb=getRecord&metadataPrefix=html&identifier=ADA342720.
[18] Paris P, Erdogan F. A critical analysis of crack propagation laws. J Basic Eng 1963;85(4):528–33.
[19] Nitta A, Kuwabara K. Thermal-mechanical fatigue failure and life prediction. Curr Jpn Mater Res 1988;3:203–22. Elsevier.
[20] Christ H-J, Jung A, Maier HJ, Teteruk R. Thermomechanical fatigue—damage mechanisms and mechanism-based life prediction methods. Sadhana 2003;28(1–2):147–65.

[21] Nikbin KM, Webster GA, Smith DJ. An engineering approach to the prediction of creep crack growth. ASME, Trans J Eng Mater Technol 1986;1986 (108):186–91.
[22] ASTM E1457. Standard test method for measurement of creep crack growth rates in metals 1; 2006. p. 1–15.
[23] Saxena A, Landes JD. Characterization of creep crack growth in metals. Advances in fracture research. In: Sixth inter-national conference on fracture. Pergamon Press; 1984. p. 3977–88. ISBN: 0080293093 9780080293097.
[24] Saxena A, Hall DE, McDowell DL. Assessment of detection rate partitioning for analyzing creep crack growth data. Eng Fracture Mech 1999;62:111–22.
[25] Nikbin KM, Smith DJ, Webster Ga. Prediction of creep crack growth from uniaxial creep data. Proc R Soc A Math Phys Eng Sci 1984;396(1810):183–97.
[26] Andrews B, Potirniche GP. Explicit and implicit lifetime assessment methods of 9Cr-1Mo steel under combined creep and fatigue loads using a strip yield model; 2015. p. 1–12. doi: http://dx.doi.org/10.1115/IMECE2014-39658.
[27] Dugdale DS. Yielding of steel sheets containing slits. J Mech Phys Solids 1960;8 (2):100–4.
[28] Shih CF. Tables of hutchinson-rice-rosengren singular field quantities. Providence, R.I.: Division of Engineering. Brown University; 1983.
[29] Special metals. Inconel Alloy HX, SMC-007(2004). www.specialmetals.com.
[30] Shih CF. Relationship between crack tip opening displacement for stationary and extensing cracks. J Mech Phys Solids 1981;29(4):305–26.
[31] MAPLE 15.01, Copyright© Maplesoft, a division of waterloo Maple Inc. 1981–2011.
[32] Sih GC, Tang XS. Micro / macro-crack growth due to creep – fatigue dependency on time – temperature material behavior. Theor Appl Fract Mech 2008;50(1):9–22.
[33] Tang KK. Fracture control over thermal – mechanical creep and fatigue crack growth in near-alpha titanium alloy. Eng Fract Mech 2013;110:300–13.
[34] Rudnev V, Loveless D, Cook RL, Black M. Handbook of induction heating, vol. 796. Marcel Dekker, New York; 2003. http://www.asminternational.org/web/hts/home/-/journal_content/56/10192/75024G/PUBLICATION.
[35] Zinn S, Semiatin S.L. Elements of induction heating: design, control and application. ASM International; 1988. ISBN: 978-0-87170-308-8.
[36] Tavakoli MH, Karbaschi H, Samavat F. Computational modeling of induction heating process. Prog Electromagn Res Lett 2009;11:93–102.
[37] Clain S, Rappaz J, Swierkosz M, Touzani R. Numerical modeling of induction heating for two-dimensional geometries. PhD Propos, vol. 1; 2015. doi: http://dx.doi.org/10.1017/CBO9781107415324.004.
[38] Dreyfuss P, Rappaz J. Numerical modelling of induction heating for two-dimensional geometries. Preprint EPFL' 2001.
[39] Quick field 6.1, copyright © 1993–2015, Tera analysis Ltd.